Structural and Chemical Evolution of an Inverse CeO_x/Cu Catalyst under CO₂ Hydrogenation: Tunning Oxide Morphology to Improve Activity and Selectivity

Jorge Moncada, ¹ Xiaobo Chen, ² Kaixi Deng, ³ Yuxi Wang, ⁴ Wenqian Xu, ⁵ Nebojsa Marinkovic, ⁶ Guangwen Zhou, ² Arturo Martínez-Arias, ⁷ José A. Rodriguez*, ^{1,3,4}

¹ Chemistry Division, Brookhaven National Laboratory, Upton, NY 11973, USA

² Materials Science and Engineering Program, State University of New York at Binghamton,
Binghamton, NY 13902

³ Department of Chemistry, Stony Brook University, Stony Brook, NY 11794, USA

⁴ Materials Science and Chemical Engineering Department, Stony Brook University, Stony Brook, NY 11794, USA

⁵ X-ray Science Division, Advanced Photon Source, Argonne National Laboratory, Lemont, IL 60439, USA

⁶ Synchrotron Catalysis Consortium, Columbia University, New York, NY 10027, USA

⁷ Instituto de Catálisis y Petroleoquímica, CSIC, Campus Cantoblanco, 28049 Madrid, Spain

* Corresponding Author: rodrigez@bnl.gov

Abstract: Small nanoparticles of ceria deposited on a powder of CuO display a very high selectivity for the production of methanol via CO₂ hydrogenation. CeO₂/CuO catalysts with ceria loadings of 5, 20, and 50% were investigated. Among these, the system with 5% CeO_x showed the best catalytic performance at temperatures between 200 and 350 °C. The evolution of this system under reaction conditions was studied using a combination of environmental transmission electron microscopy (E-TEM), in-situ x-ray absorption spectroscopy (XAS) and time-resolved x-ray diffraction (TR-XRD). For 5%CeO_x/Cu, the in-situ studies pointed to a full conversion of CuO into metallic copper with a complete transformation of Ce⁴⁺ into Ce³⁺. Images of E-TEM showed drastic changes in the morphology of the catalyst when it was exposed to H₂, CO₂, and CO₂/H₂ mixtures. Under a CO₂/H₂ feed, there was a redispersion of the ceria particles that was detected by E-TEM and in-situ TR-XRD. These morphological changes were made possible by the inverse oxide/metal configuration and facilitate the binding and selective conversion of CO₂ to methanol.

Keywords: Carbon dioxide; Hydrogen; Methanol synthesis; Hydrogenation reactions; Ceria; Copper; In-situ characterization; Microscopy

INTRODUCTION

Carbon dioxide (CO₂) is a major environmental problem due to its negative impact in the weather (global warming) and the acidification of oceans. 1,2 Chemical conversion of this molecule to oxygenates or light alkanes is a viable route to mitigate its negative effects. Cu/ZnO catalysts are frequently used in the industry to convert CO₂ into methanol.^{2,3} In a study, Lunkenbein et al. examined the behavior of the Cu/ZnO/Al₂O₃ powder catalysts under reducing conditions using high-resolution transmission electron microscopy (HR-TEM) and observed the formation of zinc oxide overlayers on top of copper.³ In this inverse oxide/metal configuration, the active phase contained graphite-like structure of ZnO which were very different from the stable wurtzite structure typically seen for bulk ZnO.³ Subsequent research using environmental transmission electron microscopy (E-TEM) has also found an inverse ZnO/Cu active phase with the zinc oxide in an amorphous structure. 4 In separate studies, highly active inverse oxide/metal catalysts for CO₂ hydrogenation have been found after depositing ZnO, CeO₂, and ZrO₂ on plain Cu(111).^{5,6,7,8} It is not clear what happens on the surfaces of these inverse oxide/metal systems under reaction conditions. 9,10,11 It is expected that they could have a unique behavior due to the special properties of oxide nanoparticles and strong oxide-metal interactions. 9-11 Since inverse oxide/metal catalysts are active for CO₂ hydrogenation, and many other chemical processes, ³⁻¹¹ it is important to explore their behavior under reaction conditions.

In this study, we focus our attention on an inverse powder CeO₂/CuO system that has shown very good performance for the preferential oxidation of CO¹² and the water-gas shift reaction¹³ and has similarities with the model CeO₂/CuO_x/Cu(111) catalyst used for CO₂ hydrogenation.⁵ In a ceria overlayer, one can have switching between 4+ and 3+ oxidation states but an oxide-metal interface is always maintained.^{5,12,13} In the case of ZnO/Cu or Cu/ZnO, under high H₂ pressures

and elevated temperatures of operation, a ZnCu alloy may be formed.^{4,14} The constant presence of an oxide-metal interface in CeO_x/Cu opens the door to interesting properties for C1 catalysis.^{5,12,13,15} The inverse oxide/metal configuration favors the formation and hydrogenation of key intermediates such as carboxyl, formate, and methoxy.^{5,15}

Here, we use a combination of environmental transmission electron microscopy (E-TEM) and two in-situ techniques (time-resolved X-ray diffraction (TR-XRD) and X-ray absorption spectroscopy (XAS)) to investigate the behavior of inverse CeO₂/CuO powder catalysts under atmospheres of H₂, CO₂, and CO₂/H₂. In these CeO_x/CuO powders, overlayer loadings of 5, 20, and 50% were investigated to change the size of the ceria component from small clusters or aggregates to medium size crystallites. ^{12,13} Our E-TEM studies point to big morphological changes that depend on the size of the ceria component and can be useful for improving catalytic activity and selectivity towards methanol synthesis. The morphology of the catalyst surface changes in different ways in the presence of H₂ or H₂/CO₂ gas mixtures, highlighting the importance of the interaction of CO₂ with the oxide nanoparticles.

METHODS

Preparation of the catalysts

Inverse CeO_x/CuO catalysts containing 5, 20, and 50% of ceria were prepared following the methodology used in previous studies by the authors and described in reference 12, employing a reverse microemulsion method containing n-heptane, Triton-X-100, and n-hexanol as organic solvent, surfactant, and cosurfactant in a volume proportion of 1.00/0.20/0.21 of the mentioned components, respectively. Copper nitride was added to this microemulsion (volume proportion

1.00/0.20/0.21/0.11), plus additional tetramethyl ammonium hydroxide (TMAH) to induce precipitation of the inorganic precursor, followed by drying at 120 °C and calcination under air at 500 °C to generate the copper oxide substrate. Ceria was deposited in a second step on the CuO particles by introducing the particles in a microemulsion of similar characteristics where cerium nitrate has been added in its aqueous phase and finally using a TMAH microemulsion to precipitate the cerium on the CuO particles followed by drying at 120 °C and calcination under air at 500 °C. 12 By changing the molar concentration of the cerium nitrate in the second synthesis step, we were able to vary the concentration of ceria on the copper oxide substrate. 12,23 Optimal performance was found at ceria weight loadings below 10% when small ceria nanostructures (< 5 nm in size) were present on the copper oxide substrate. At ceria weight loadings above 10%, the size of the ceria particles grew fast, and their behavior got closer to that of bulk ceria. The properties of the CeO_x/CuO catalysts were characterized using a combination of TEM, XPS, XANES and XRD. 12,13 The as prepared samples exhibited an inverse CeO₂/CuO configuration, with nanostructures or crystallites of ceria on top of a copper oxide support. 12,13

Catalytic tests:

A set of experiments examining the hydrogenation of CO₂ was done in a fixed-bed stainless-steel flow reactor loaded with 0.2 g of the powder catalysts (400-800 microns) at temperatures between 200 and 300 °C with a total pressure of 20 atm (75% H₂ plus 25 % CO₂, flow rate 5 mL/min). The system was initially pressurized with the reaction mixture of CO₂/H₂ at 25 °C and then the temperature was raised to a desired final value in the range of 200-300 °C with the total pressure adjusted to a value of 20 atm (75% H₂ plus 25 % CO₂). No significant pressure drop was detected along the reactor. Gas and liquid (collected in a cold trap) products were analyzed using a gas chromatographer (equipped with a thermal conductivity (TCD) detector and two flame

ionization (FID) detectors) after careful calibration against standards. The accuracy of the analysis was also verified by comparing to test measurements with an internal standard in the reaction feed (CO₂/H₂/N₂). H₂, CO₂, and CO were monitored by the TCD detector, while the FIDs were used to look for the formation of CH₃OH and other oxygenates plus CH₄. Only CO and CH₃OH were detected as products. For each CeO_x/CuO catalyst, we performed three independent measurements starting with fresh samples. The results for each catalyst composition showed minor variations. The reported values of activity and selectivity (including small error bars) come from an average of these three measurements. The ceria nanostructures in the inverse CeO_x/CuO configuration facilitate the splitting of the H₂ molecule and the reduction of CuO.^{5,9,13} This fast reaction with hydrogen determined the chemical composition of the catalysts. In a relatively short period of less than 5 minutes, at the elevated temperatures used for CO₂ hydrogenation (200-300 °C), the results of XPS, XANES and XRD (see below) indicate that the CeO_x/CuO catalysts reached their final compositions, that involved Ce₂O₃/Cu for 5%CeO_x/CuO and CeO₂/Cu for 20% and 50%CeO_x/CuO, and, after stablishing steady state, no significant variations in activity or selectivity were seen in the following 100 hours. The reported values are those found under steadystate conditions. The conversion (Con) and selectivity (Sel) are defined as:

$$Con = (nCO_{2,in} - nCO_{2,out}) / nCO_{2,in}$$

$$Sel = n_{CH3OH,out} / (n_{CO2,in} - n_{CO2,out})$$

Experiments examining the hydrogenation of CO₂ were also performed in a flow reactor at atmospheric pressure with a ratio 3:1 for H₂ and CO₂. In these studies, measurements were done

at 250 and 350 °C. Mass spectrometry was used to analyze the gas composition in the outlet of the reactor following masses for possible products such as CO, CH₃OH, and CH₄. Under atmospheric pressures, the only product detected in the mass spectrometer was CO. The decrease in the CO₂ signal under catalytic conditions was used to estimate the conversion of this molecule.

In-situ characterization

Transmission Electron Microscopy: The morphology of the catalysts was examined at the Center for Functional Nanomaterials (CFN) at Brookhaven National Laboratory (BNL). The high-angle annular dark-field (HAADF) – scanning transmission electron microscopy (STEM) images and the corresponding energy-dispersive X-ray spectroscopy (EDS) mapping were captured using FEI Talos F200X operated at 200 kV and equipped with a four-quadrant EDS detector. In-place HRTEM observations of the dynamic behaviors of catalysts in reducing and CO₂ hydrogenation gas ambient were performed using an image-corrected environmental TEM (FEI Titan 80-300) equipped with a differential pumping system.

In-situ X-ray Absorption Spectroscopy: The X-ray Absorption Near Edge Structure (XANES) spectra for the evaluated catalysts were collected at the 7-BM Quick X-ray Absorption and Scattering (QAS) beamline of the National Synchrotron Light Source II (NSLS-II) at BNL. The evaluated powder catalysts were drop casted (~ 1 mg) onto an aluminum foil and the foil was mounted in a Nashner-Adler cell. The reported Ce L_{III}-edge and Cu K-edge XANES spectra were collected in the fluorescence mode using a PIPS detector. Following the working procedures of the QAS beamline, the Ce and Cu edges were calibrated using Cr and Cu foils as standards, respectively. Datasets were analyzed using the Athena software package.

In-situ X-ray Diffraction: The data of time-resolved X-ray diffraction were collected at the 17-BM-B Structural Science (XSD-SRS) beamline of the Advanced Photon Source (APS) in Argonne National Laboratory (ANL) using an area detector Varex 4343CT (150-micron pixel size). The x-ray wavelength of the beam was 0.24012Å with a spot size focused at 300μm x 300μm. The catalysts were evaluated in a Clausen cell by using a quartz capillary with a 0.9 mm ID and 1.1 OD dimensions. The powder sample (2-3 mg) was placed in the middle of the capillary using quartz wool plugs at the top and bottom of the catalyst bed. The datasets obtained were analyzed by using the GSAS-II software package.

Ex-situ X-ray photoelectron spectroscopy: In a reaction cell, the CeO_x/CuO powders were exposed to a gas mixture (75% H_2 plus 25 % CO_2) at pressures of 1 Torr, 1 atm and 20 atm and temperatures in the range of 100-250 °C for five minutes. After this treatment, the gases were pumped out and the samples were transferred (without exposure to air) to an adjacent ultra-high vacuum chamber equipped with instrumentation for X-ray photoelectron spectroscopy (XPS). XPS spectra were acquired using a regular Mg K α source with an Omicron high-resolution hemispherical analyzer. Post reaction characterization of the catalysts' chemical state was done by examining the Ce 3d and Cu $2p_{3/2}$ XPS core-levels and the Cu L_3VV Auger features.

RESULTS AND DISCUSSION

Performance of the CeO₂/CuO catalysts: Effect of ceria loading

In this study, the catalytic performance of CeO_x/CuO powders with ceria loadings of 5, 20, and 50% was investigated. The catalysts were evaluated under CO₂ reduction conditions with a ratio of 3:1 for H₂ and CO₂. Methanol and CO were the only products detected. At high pressures (20

atm), a close to 90% selectivity to methanol was found for the 5%CeO_x/CuO_y catalyst at low CO₂ conversion values (Figure 1). A high selectivity (> 80%) was also seen when the CO₂ conversion was significantly increased by raising the reaction temperature (Figure S1). Essentially, it did not change after a period of 100 hours of operation (Figure S2). This extremely high selectivity makes

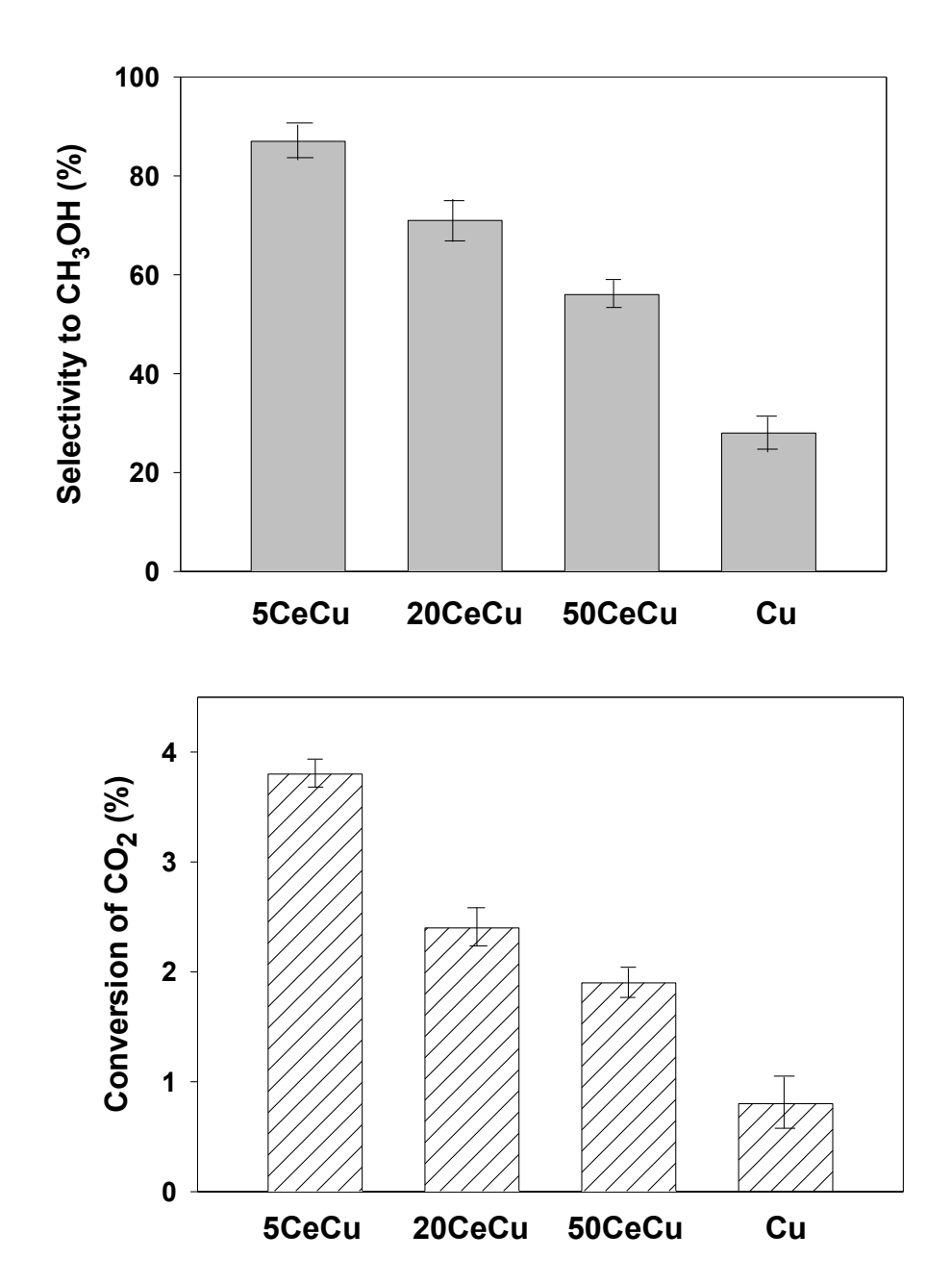


Figure 1. (top) Selectivity to CH₃OH and (bottom) CO₂ conversion data obtained at 20 atm and 250 °C for the three tested CeO_x/Cu catalysts with 5, 20 and 50% CeO_x. Plain copper was included as a reference.

this powder catalyst special. 8,16,17,18 For a conventional Cu/ZnO/Al₂O₃ catalyst, used in many industrial applications, the selectivity to methanol is in the range of 30-60% when tested under similar reaction conditions. 16,17,18 At atmospheric pressures, only reverse water-gas shift (CO₂ + H₂ \leftrightarrow CO + H₂O) reaction products were observed (Figure S3). The absence of methoxy or methanol was expected as methanol production is known to happen at pressures much higher than 1 atm. 5,17,19 As shown in Figures 1 and S3, independently of the total pressure and main reaction, the studied catalysts show a similar reactivity trend towards product formation with the best performance seen for 5% CeO_x/CuO_y.

Interestingly, in Figures 1 (bottom) and S3, an inverse catalyst with a medium loading of 20% of CeO_x is not very active. For these CeO_x/CuO_y systems, we saw very good catalytic performance only for weight ceria loadings below 10%. The performance results as a function of ceria loading suggest that the formation of a ceria-copper interface is important, but the ceria must have special properties in that interface that are only possible when the oxide is present as small nanoparticles.

After performing the CO₂ hydrogenation reaction at 20 atm and 250 °C, the chemical composition of the catalysts was examined with XPS (Figures S4-S6). The data for the Cu $2p_{3/2}$ XPS core level (Figure S5) and the Cu L_3VV Auger features (Figure S6) point to a full transformation of CuO into metallic copper.²⁰ In an inverse CeO_x/CuO configuration, neither CuO nor Cu₂O are stable under H₂ or the CO produced by CO₂ dissociation.^{5,9,13} The main oxidation state of ceria depends on the loading of the oxide on copper. The 5%CeOx catalyst exhibits a Ce 3d XPS line shape (Figure S4) identical to that of Ce³⁺ or Ce₂O₃ species.²¹ Initially, the as-prepared 5%CeOx/CuO catalyst contained mainly Ce⁴⁺ cations, but these species were not stable, and even

exposure to a relatively small pressure of 1 Torr of CO_2/H_2 induced a massive $Ce^{4+} \rightarrow Ce^{3+}$ transformation (Figure S7). In the cases of 20% and 50% CeOx/CuO, this transformation did not occur and after reaction these catalysts displayed Ce 3d XPS spectra characteristic of Ce^{4+} or CeO_2 (Figure S4).²⁰ As we will see below, the ceria particles in 20% and 50% CeOx/CuO are already too big and display a behavior similar to that of bulk ceria.

To gain insights into the structural and electronic properties of CeO_x/CuO that determine the activity of this catalyst, systematic in-situ characterization studies with several techniques (TEM, XANES, and XRD) were performed during (i) H₂ pretreatment, (ii) after exposure to CO₂, and (iii) under CO₂ conversion. Post-reaction characterization with XPS indicated that key changes in chemical state for the CeO_x/CuO catalysts at the elevated temperatures (> 200 °C) used in CO₂ hydrogenation already occur under a total pressure of 1 Torr (Figures S7-S8). Thus, for the highly active 5%CeO_x/CuO catalyst in Figures 1 and S3, the elemental composition is the same (Ce₂O₃/Cu) during the reverse water-gas shift reaction and methanol synthesis.

Catalyst dynamics under reducing conditions: Chemical and morphological changes induced by reaction with H₂,

Metal/oxide catalysts used in CO₂ hydrogenation usually are activated by pre-treatment in H₂ at 350-450 °C.^{3,5-7,17-19} CeO_x nanostructures deposited on copper oxide facilitate the dissociation of H₂ and the subsequent reduction of copper.^{5,9,13} After comparing with XRD patterns reported for CuO and Cu,^{22,23,24} our results of in-situ time-resolved XRD indicated that upon exposure to H₂, the CuO component in the catalysts was rapidly reduced, in less than five minutes, to metallic copper (Figure 2), mimicking the behavior previously seen for the CeO_x/CuO_y/Cu(111) model system and powder catalysts that contained a CeO₂-CuO interface,^{5,12,13} and in agreement with our XPS studies in Figures S5, S6 and S8. The results of XANES also pointed to a reduction of the

copper oxide (Figure 3b), yielding spectra with photon energies and a line shape that closely matched that of metallic Cu (Figure S9 and refs 13 and 23). In the corresponding Ce L_{III} edge spectra (Figure 3a), we found the typical line-shape for Ce³⁺ or Ce₂O₃²⁵ in the 5%CeOx/CuO catalyst and a mixture of Ce³⁺ and Ce⁴⁺ in the 20% and 50% CeO_x/CuO catalysts. For these two catalysts, the XANES analysis in Figure S10 points to systems where at least 60 % of the ceria is in a 4+ oxidation state. In XANES, we may be detecting bulk components of Ce³⁺ and Ce⁴⁺ not

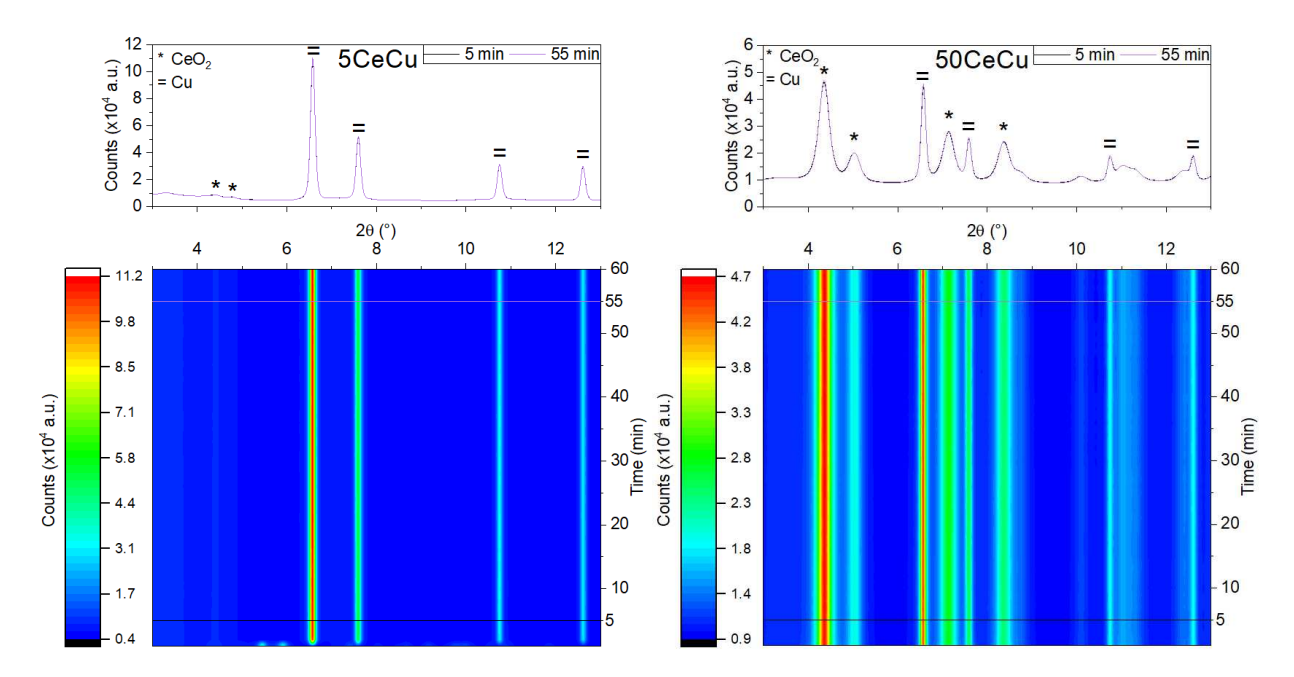


Figure 2. In-situ XRD of the 5%CeO_x/Cu (left side) and 50%CeO_x/Cu (right side) catalysts under reducing conditions (20% H₂/Ar, 400 C, 1h). At the top of the figure, overlayed diffraction patterns are shown close to the beginning (5 min) and end (55 min) of the experiment. They are identical indicating that the chemical transformations occur in less than five minutes. The diffraction pattern for the CuO phase (JCPDS 45-0937) has disappeared and only a metallic Cu phase (JCPDS 04-0836) is observed.²²⁻²⁴

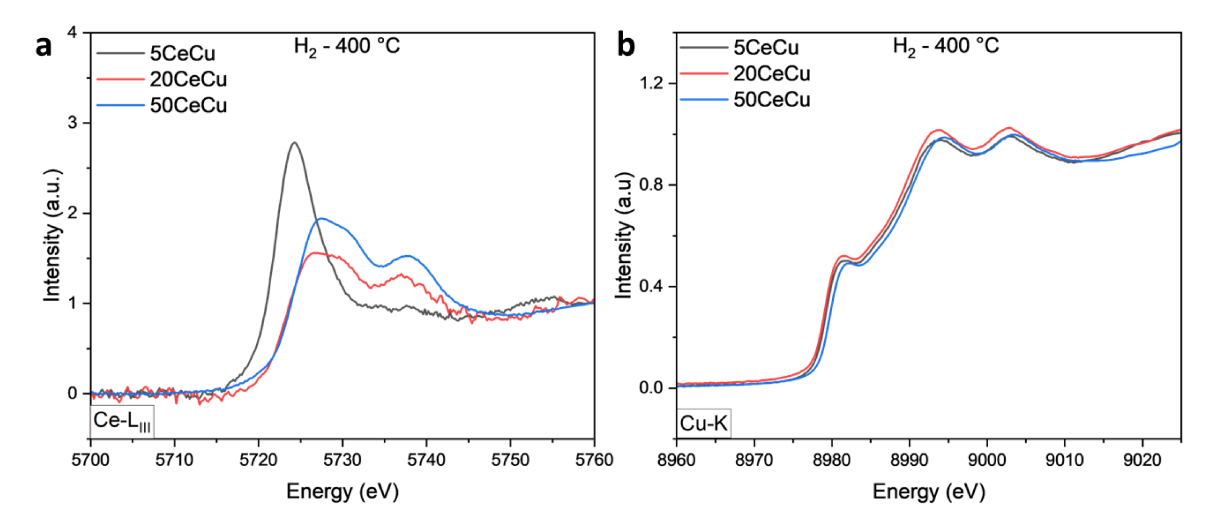


Figure 3. In-situ XANES data for the CeO_x/CuO catalysts under reduction conditions (20% H₂/Ar, 400 °C, 1h). (a) Cerium L_{III} and (b) copper K edge. The 5% CeO_x/CuO system transforms into a Ce_2O_3/Cu catalyst. ^{13,22,24} A detailed comparison with standards (refs 22 and 23 and Figure S9) and analysis of the Ce L_{III} XANES data for 20 and 50% CeO_x/Cu are presented in Figure S10.

seen in a mainly surface-sensitive technique like XPS (Figure S7).

By using STEM, EDS, and EELS (Figure 4 and S11), it could be confirmed that the ceria nanoparticles were dispersed on a reduced copper support generated by pre-treatment of the asprepared CeO_x/CuO_y catalysts in H₂. Agglomeration of the ceria component (i.e. three-dimensional (3D) growth and lack of copper wetting) was clearly seen when the oxide loading was increased to 20 and 50%. The EELS measurements for the Ce M4 and M5 edges in Figure 4 show

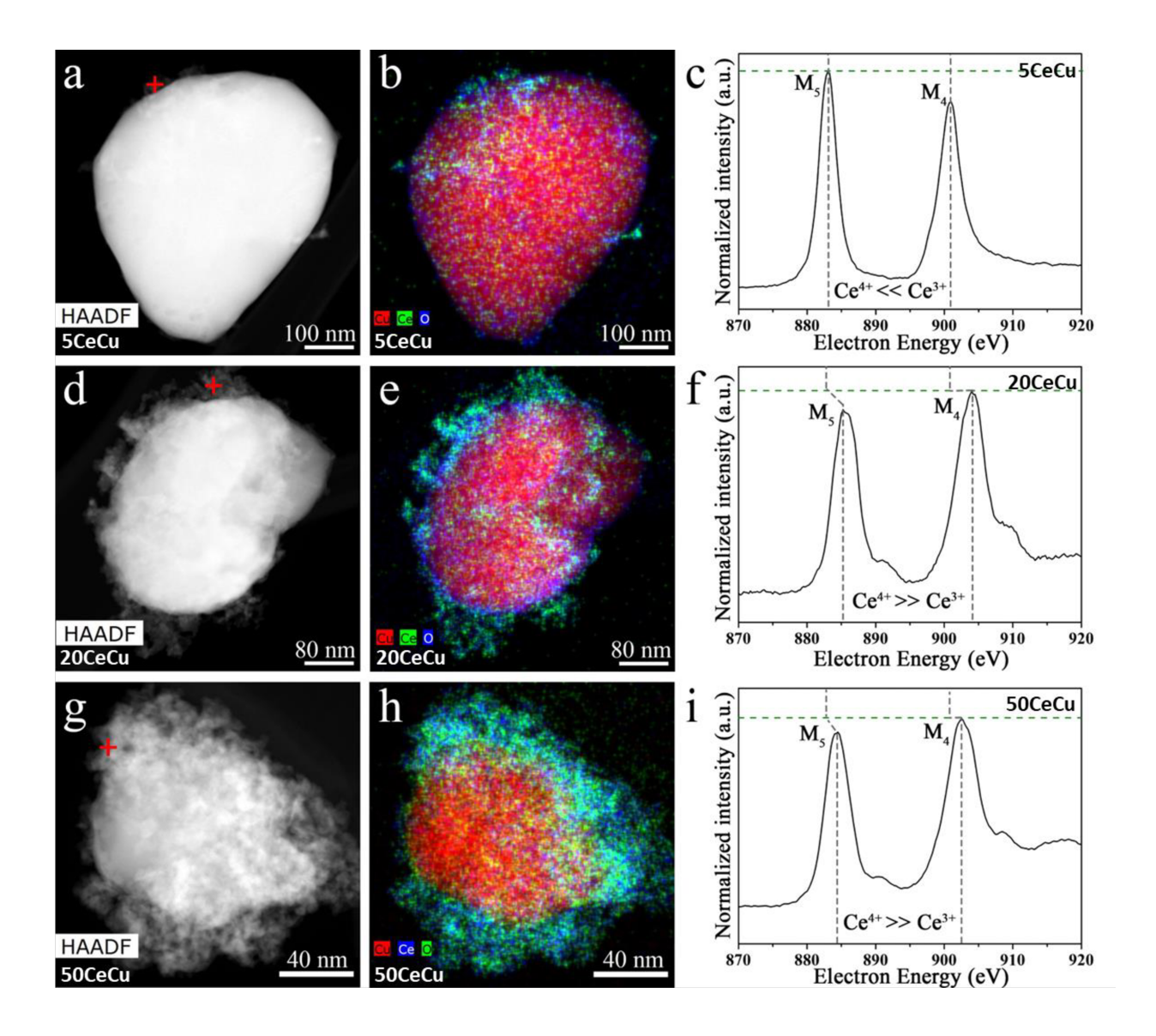


Figure 4. STEM images (a, d, g), combined EDS maps of Cu, Ce and O (b, e, h), and EELS spectra (c, f, i) for the 5%CeO_x/Cu (top), 20%CeO_x/Cu, and 50%CeO_x/Cu (bottom) catalysts under reducing conditions (5mTorr of H₂, 450 °C). The ceria growth mode and main oxidation state are clearly modified when going from a weight loading of 5 to 20 or 50%.

typical features for ceria compounds 26 and are consistent with the fact that Ce^{3+} is the dominant species in the 5%CeO_x catalyst, with Ce^{4+} being the main component for the 20% and 50% CeO_x catalysts.

The results in Figure 2 point to a crystalline phase of ceria in 50%CeO_x/CuO that is not seen in the case of 5%CeO_x/CuO. This is consistent with the STEM-EDS elemental maps in Figure 4,

showing a much stronger Ce/O intensity for 50%CeO_x/CuO (Figure 4h) than that from the 5%CeO_x/CuO sample (Figure 4b). Using E-TEM, we were able to track local structure and morphology changes in the catalysts. To evaluate the catalyst in its reduced state, the sample initially underwent an ex-situ reduction pretreatment in 20% H₂/Ar at 400 °C and atmospheric pressure. After this step, the sample was transferred to the E-TEM cell and taken again to the reducing conditions at a lower total pressure (5 mTorr of H₂, 450 °C). Multiple tests were done to verify that the images in Figure 5 are not a consequence of electron beam irradiation.

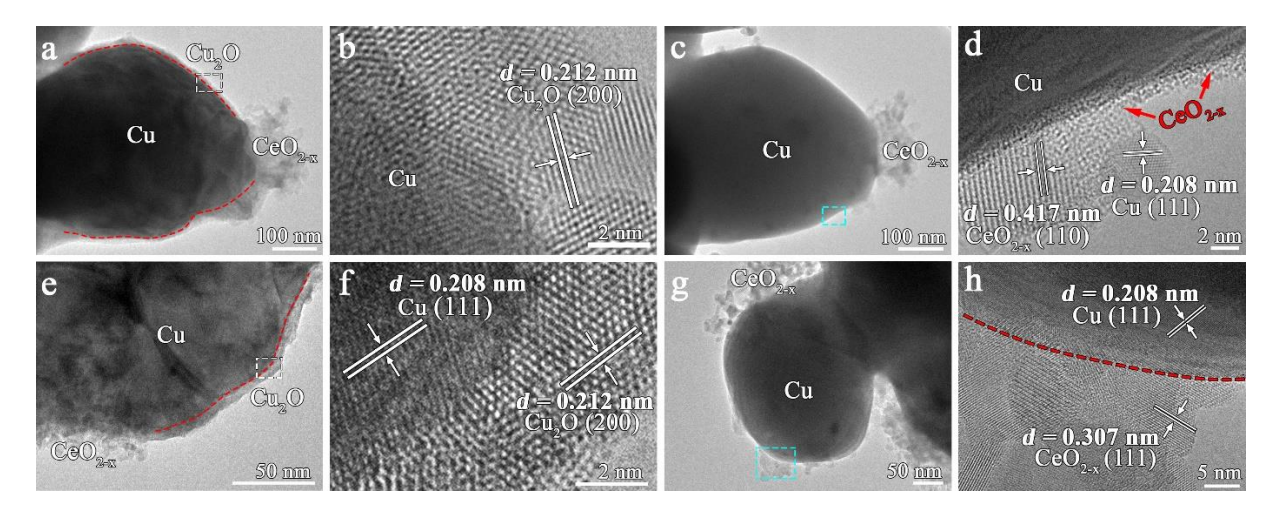


Figure 5. E-TEM images for the (a-d) $5\%\text{CeO}_x/\text{Cu}$ and (e-h) $50\%\text{CeO}_x/\text{Cu}$ catalysts under the ex-situ prereduced (20% H₂/Ar, 1bar, 450 °C) conditions: (a-b, e-f) vacuum and (c-d, g-h) 5 mTorr H₂, 450 °C. The H₂ dosing results in the decomposition of the Cu₂O layer (formed due to the air exposure before loading into the TEM column) (a \rightarrow c; e \rightarrow g) and surface dispersion of ceria in the case of $5\%\text{CeO}_x/\text{Cu}$.

As shown in Figure 5 c-d, under reducing conditions, which should lead to the formation of Ce₂O₃ and metallic Cu in 5% CeO_x/CuO (Figures 2-4), there is a coexistence of half-ordered and disordered structures, and an amorphous ceria layer of ~ 2 nm in thickness is formed on some surface areas of the copper particle. Therefore, a synergistic effect present at low loading could be helping to disperse this Ce₂O₃ phase. Such a phenomenon was not seen for the 50%CeO_x/Cu catalyst that initially had larger sizes on ceria structures (Figures 2 and 4h) dispersed over the copper (Figure 5e,g). For this system, pre-treatment in H₂ did not lead to a massive reduction of

the Ce⁴⁺ (Figures 3a and 4i) and most of the ceria remained in a crystalline phase as confirmed by time-resolved XRD (Figure 2). Thus, the initial state (crystalline vs. amorphous) of the oxide particles in the inverse oxide/metal configuration does matter.

Adsorption and dissociation of CO2: Reoxidation of the CeOx/Cu catalysts

In another set of experiments, we investigated the interaction of CO_2 with the reduced CeO_x/Cu catalysts using in-situ time-resolved XRD (Figure 6 and S12) and XANES (Figures 7). The results point to a partial dissociation of the CO_2 molecule ($CO_{2,gas} \rightarrow CO_{gas} + O_{ads}$) that oxidizes metallic copper and Ce^{3+} cations present in the catalysts. In Figure 6, the time-resolved XRD data show a progressive reduction in the diffraction lines for Cu with the growth of lines for $Cu_2O.^{22,23}$ The line-shape of the Cu K-edge shifts from metallic (Figure 3) to that of Cu_2O (Figures 7b and S9b). At the Ce L_{III} edge (Figure 7a), there was a clear increase in the features for Ce^{4+} around 5736.4 eV that led to a decrease of the Ce^{3+}/Ce^{4+} ratio in the catalysts. Thus, it was clear that both components in the ceria-copper interface were reactive toward CO_2 . In contrast, the dissociative sticking of CO_2 on pure extended surfaces of copper is very low CO_2 and extended surfaces of ceria usually react with CO_2 to form plain carbonates.

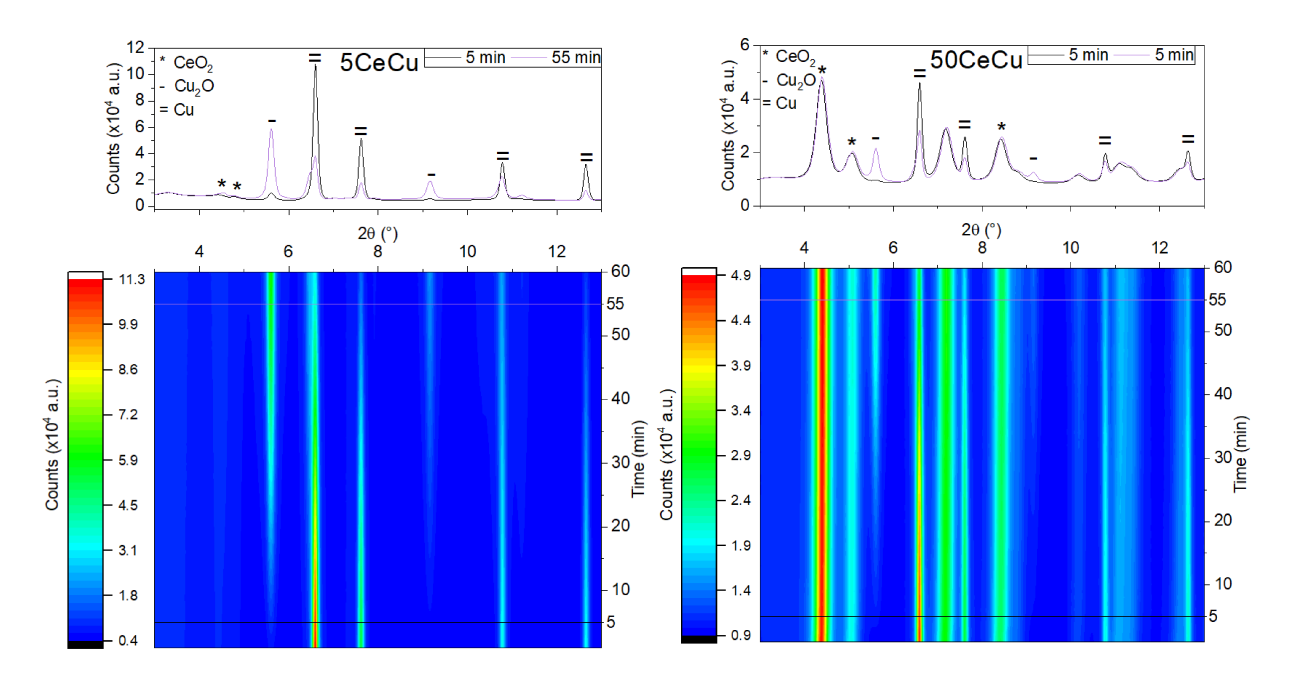


Figure 6. In-situ XRD of the reduced 5%CeOx/Cu (left side) and 50%CeO_x/Cu (right side) catalysts under CO₂ exposure (20% CO₂/Ar, 250 C, 1h). At the top, overlayed diffraction patterns are shown close to the beginning (5 min) and end (55 min) of the experiment. There is a progressive reduction of the Cu phase (JCPDS 04-0836) and formation of Cu₂O (JCPDS 05-0667)²⁴ by reaction of CO₂ with metallic copper.

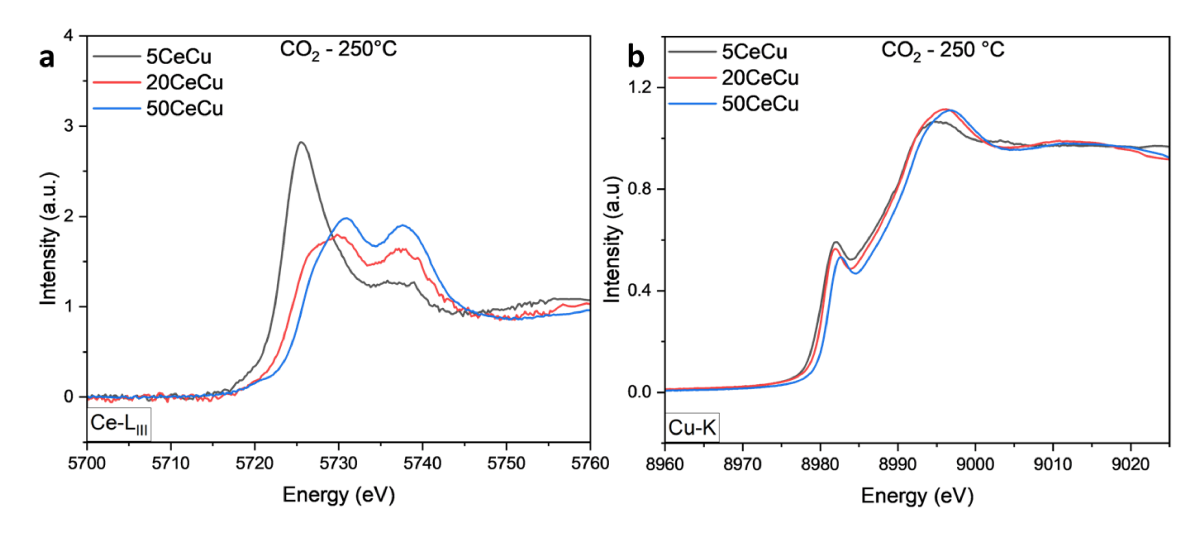


Figure 7. In-situ XANES spectra for the reduced CeO_x/Cu catalysts under reaction conditions with 20% CO_2/Ar (250 C, 1h). (a) Cerium L_{III} edge and (b) copper K edge. A comparison to standards (refs 23 and 23 plus Figure S9) indicates the conversion of Cu to Cu_2O and an oxidation of Ce^{3+} centers.

Catalyst dynamics under CO₂ hydrogenation: Chemical and morphological changes

The oxidative power seen for CO₂ on the reduced CeO_x/Cu catalysts (Figures 6 and 7) was not found when these samples were exposed to a H₂/CO₂ reaction feed with a 3:1 ratio (Figures 8, 9, and S11-S12), identical to the one used in the catalytic tests of Figures 1 and S1-S3, or even when changing to a plain 1:1 ratio. Furthermore, the catalysts compositions derived from the in-situ studies with time-resolved XRD and XANES match those found in post-reaction characterization with XPS (Figures S4-S8). Under an H₂/CO₂ atmosphere, the active phase of the catalysts contains metallic copper (Figures 8, S5 and S6). The relative concentrations of Ce³⁺ and Ce⁴⁺ cations

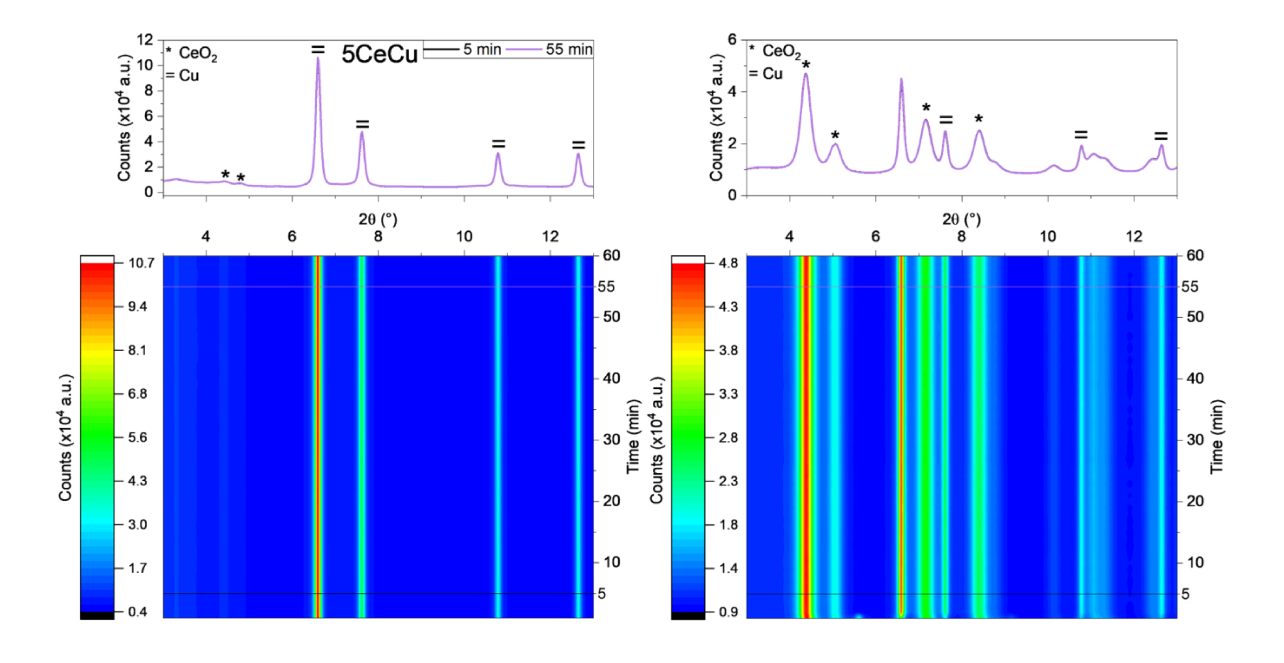


Figure 8. In-situ XRD of the 5%CeO_x/Cu (left side) and 50%CeO_x/Cu (bottom) catalysts under 3H₂:CO₂ exposure (250 C, 1h). At the top, overlayed diffraction patterns are shown close to the beginning (5 min) and end (55 min) of the reaction studies. The lack of change in the diffraction patterns indicates that all the changes in the chemical composition of the catalyst occurred in less than five minutes. The diffraction pattern for the CuO phase (JCPDS 45-0937) has disappeared and only a metallic Cu phase (JCPDS 04-0836) is observed.²²⁻²⁴

depended on the ceria loading. The graphs in Figure 9 summarize the XANES and XRD results for the 5%CeO_x/CuO catalyst. The active phase for the most active system in Figure 1 and S3

essentially contains Ce₂O₃ dispersed on metallic copper. This was valid at total pressures ranging from 1 Torr to 20 atm (Figures S7 and S8). For 20% and 50% CeOx/CuO, the active phases contained mainly CeO₂ on metallic copper (Figures 8, S4-S6, and S13). The in-situ experiments and post-reaction characterization showed a clear correlation linking the Ce₂O₃ overlayer present in the 5%CeO_x/CuO powder and high catalytic activity as seen previously for a Ce₂O₃/CuO_x/Cu(111) model system.⁵

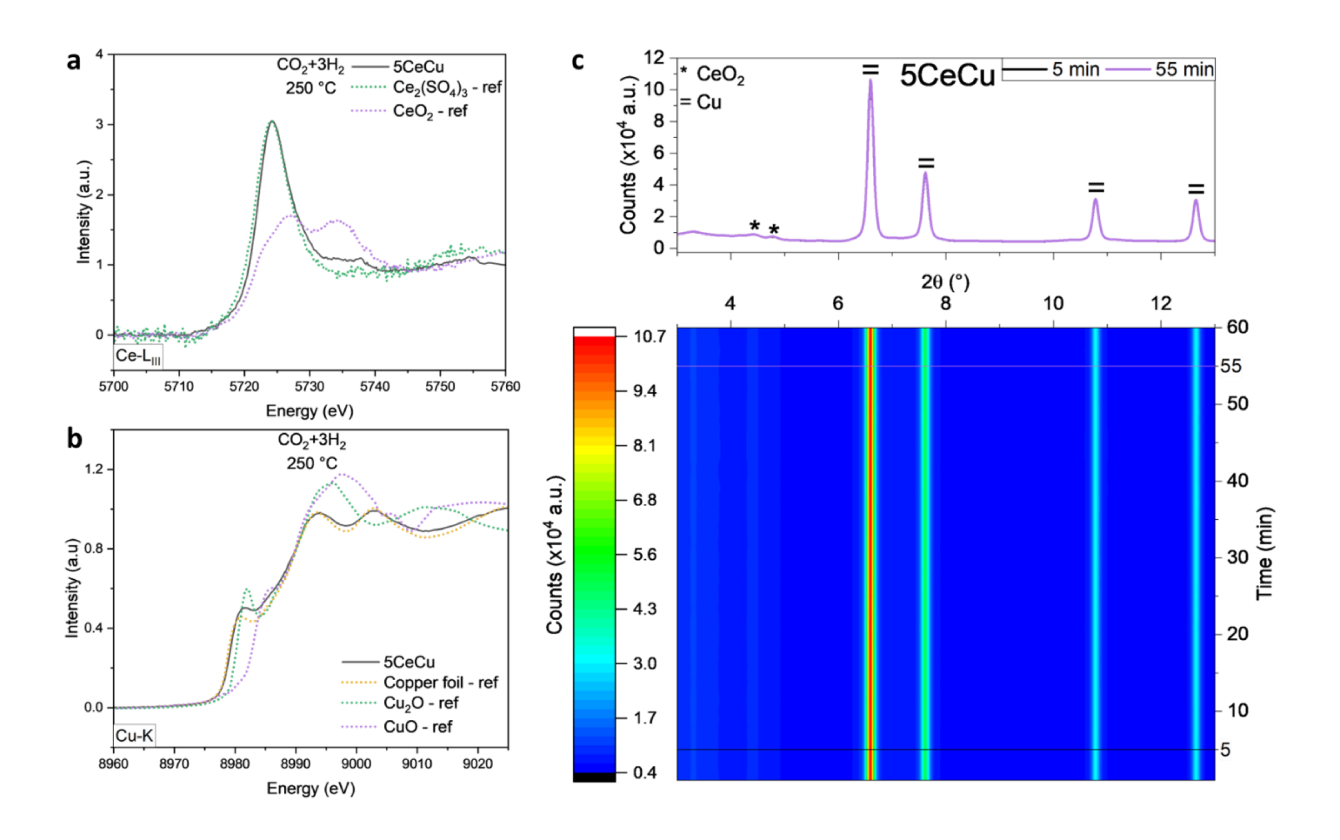


Figure 9. In-situ XANES spectra at the Ce $L_{\rm III}$ (a) and (b) Cu-K edges for the reduced 5%CeO_x/Cu catalyst under reaction conditions with $3H_2$:CO₂ (250 °C, 1h). The XANES line-shapes match those seen for $Ce_2O_3^{24}$ and metallic Cu.²³ (c) Corresponding in-situ XRD data for the 5%CeO_x/Cu catalyst under reaction conditions with $3H_2$:CO₂ (250 °C, 1h). At the top of part c, overlayed diffraction patterns are shown close to the beginning (5 min) and end (55 min) of the reaction studies. The lack of change in the diffraction patterns indicates that all the changes in the chemical composition of the catalyst occurred in less than five minutes. The diffraction pattern for the CuO phase (JCPDS 45-0937) has disappeared and only a metallic Cu phase (JCPDS 04-0836) is observed.²²⁻²⁴

E-TEM was used to study changes in the morphology of a 5%CeO_x/CuO catalyst under different reaction environments. In the images coming from E-TEM (Figure 10), there is a change in the morphology of the system with respect to that seen under pure H₂ (Figure 10a) or for a pristine CeO_x/CuO systems. ^{12,13} These images illustrate the tremendous effect that the chemical environment can have on the surface structure of an inverse oxide/metal catalyst. Here, an amorphous layer of Ce₂O₃ is well dispersed over the Cu substrate. We verified that these morphological changes were not an effect due to irradiation by the electron beam. The flattening of the ceria overlayer was seen all over the catalyst surface in fresh regions that were barely exposed to the electron beam. As soon as small amounts of CO₂ were introduced in a gas environment rich in H₂, flattening and redispersion of the ceria was seen.

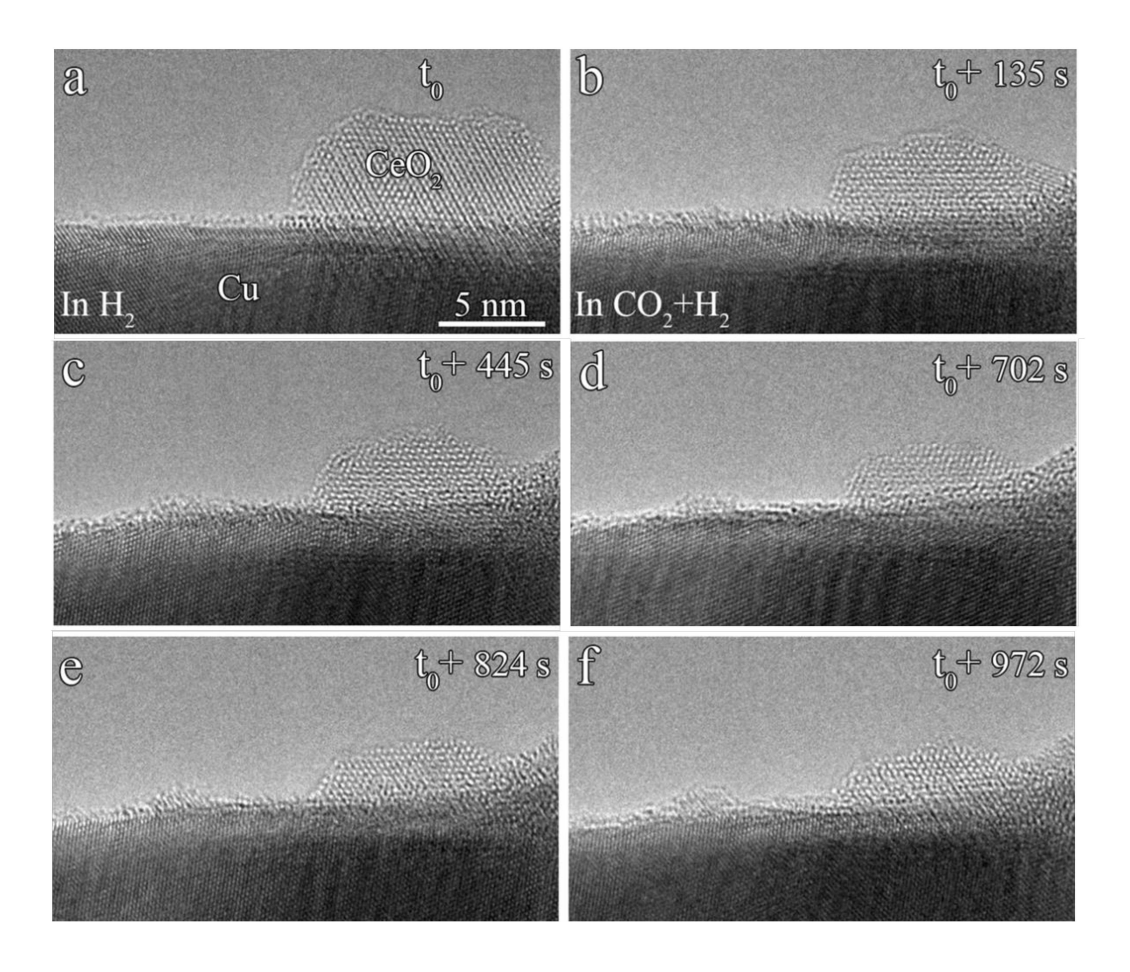


Figure 10. E-TEM images for a 5%CeO_x/Cu catalyst after switching from (a) reducing to (b-f) CO₂ hydrogenation conditions (5mTorr of CO₂, 5mTorr of H₂, 250 °C). All the images were collected on the same spot of the sample.

The substantial changes in chemical state and morphology seen for the 5%CeO_x/Cu system are probably linked to the superior catalytic activity and selectivity reported in Figures 1 and S1-S3. Post-reaction characterization using C 1s XPS showed a distinct reaction intermediate on the surface of the 5%CeO_x/Cu catalyst (Figure 11). In the measured XPS spectra, the main peaks could be assigned to methoxy (287 eV) and a mixture of formate and carbonate species (290 eV). 27,28,29,30 Only on the surface of the 5%CeO_x/Cu catalyst, one could see a significant amount of CH₃O formed by reaction of CO₂ and H₂ (Figure 11). This species is the ideal intermediate for the generation of methanol and should transform into methanol while heating under an atmosphere of H₂.^{5,30,31} The systems with 20 and 50% of CeO_x did not exhibit significant changes in their chemical state and morphology under a CO₂/H₂ feed and could not develop the type of active sites necessary for the effective binding of CO₂ and its conversion of CH₃O. Thus, on the catalyst with a relatively large loading of ceria, CO₃/HCOO species were the main adsorbates (Figure 11). None of these is a good intermediate for a selective $CO_2 \rightarrow CH_3OH$ transformation.^{5,30,31} For example, the formate group usually yields H₂ and CO₂ upon heating and is not as efficient as CH₃O in the selective production of methanol.^{31,32}

Morphology and catalytic activity in inverse oxide/metal catalysts

Previous E-TEM studies have reported changes in the configuration of metal/oxide (Cu/ZnO and Ni or Pt on TiO₂) catalysts upon reaction with H₂ that led to structural transformations and an inverse oxide/metal configuration that is essential for good catalytic performance.^{3, 4,33,34} CO is also known to induce morphological changes.^{35,36,37,38} The morphological changes in a commercial

Cu/ZnO/Al₂O₃ catalyst under CO₂ hydrogenation conditions^{3,4} can be very complex, copper-zinc oxide interfaces that have different crystallinity can coexist, and interactions with the alumina

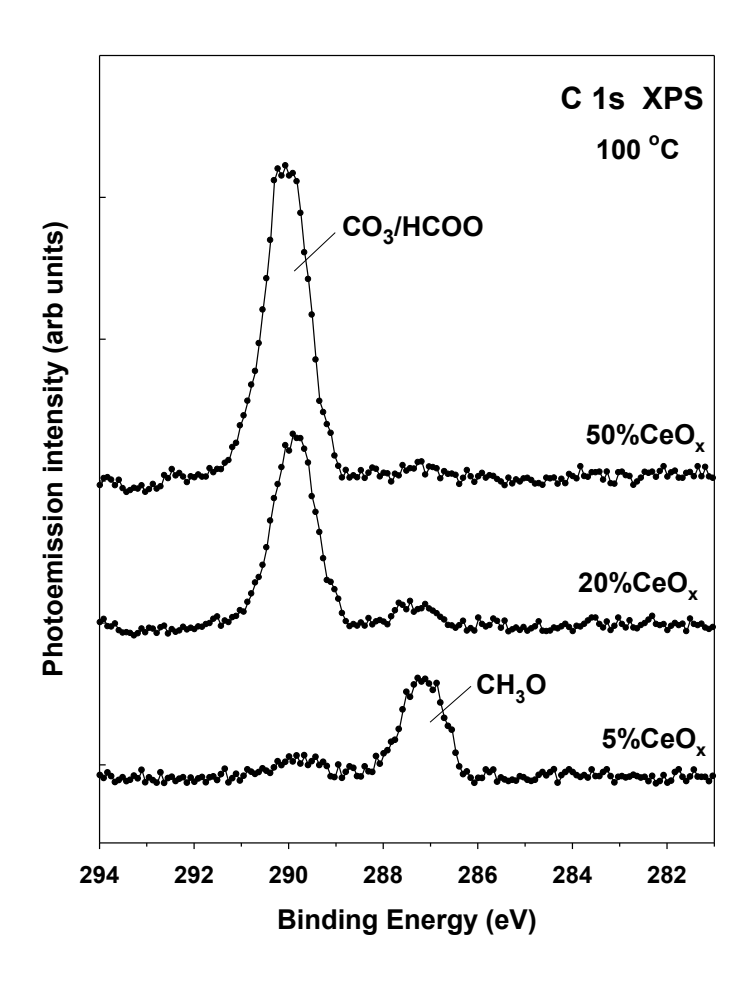


Figure 11. C 1s XPS spectra collected after exposing the CeO_x/Cu catalysts to a gas mixture with a total pressure of 20 atm (75% H_2 plus 25 % CO_2) at a temperature of 100 °C for five minutes.

support complicate things.⁴ For shape-selected nanocubes of Cu₂O supported on ZnO,³⁹ there is reduction of the copper oxide and the produced metallic copper is covered by a layer of ZnO. Since we start with an inverse oxide (CeO_x)/metal (Cu) system, the morphological changes seen in Figure 10 have not been detected in microscopy studies for other catalysts where the system starts with a metal/oxide configuration and ends as an inverse oxide/metal catalyst.^{3, 4, 32-34,38} In our system, the

amount of oxide is very small (limited) when compared to those seen after working with commercial Cu/ZnO/Al₂O₃ catalysts^{3, 4} and Cu₂O/ZnO powder models.³⁹ In Figures 4i and 10, we are truly dealing with oxide nanostructures in contact with a metal substrate. Its special chemical (Figure 11) and catalytic (Figures 1 and S1) properties are a consequence of this characteristic.^{10,11} The strong bonding interactions of two-dimensional ceria with metallic copper ⁴⁰ favor the dispersion of the small ceria crystallites in 5%CeO_x/Cu. In addition, when this ceria is dispersed on copper, it interacts better with CO₂ and subsequent intermediates in the hydrogenation process.⁵ The energy released by the formation of bonds with copper and the adsorbed molecules is the driving force for the structural transformation seen in Figure 10 under a CO₂/H₂ mixture. The size of the ceria particles is critical. At ceria concentrations above 10%, they gain stability when they grow, and then the energy released by bonding to copper and adsorbates is not enough for restructuring the ceria lattice.

Calculations based on density-functional theory (DFT) have been used to examine the hydrogenation of CO₂ on Ce₂O₃/Cu(111).⁵ The theoretical calculations showed the important role played by Ce³⁺ centers and the binding and transformation of CO₂ occurred at the copper-Ce₂O₃ interface.⁵ Two factors contributed to the special catalytic properties of this system: The ultra-thin ceria layer has specific properties, not seen for the bulk oxide, that get chemically enhanced by interaction with the metal.⁴⁰ In the DFT studies, the inverse oxide/metal configuration facilitated the conversion of typical intermediates seen in the hydrogenation of carbon dioxide (CO₂⁵, HOCO, CHO, CH₂O, CH₃O).⁵ The transformation of these species occurs on the ceria-copper interface through transition states that have barriers smaller than 16 kcal/mol. A conversion that is very difficult to achieve when CeO₂ is in a bulk state.^{5,40} Thus, the morphological changes seen in Figure 10 maximize the dispersion of small ceria aggregates on the copper substrate, produce unique

chemical properties (Figure 11), and probably lead to high catalytic activity/selectivity (Figures 1 and S1).

It is known that small nanoparticles of ZnO, ZrO₂, InO_x and SnO_x dispersed on copper also induce high catalytic activity for CO₂ reduction.^{3-6,41,42} They can be very active for the splitting of H₂ and the binding/conversion of CO₂.^{6,9,41,42} The changes in composition and morphology seen in this study for the 5%CeO_x/Cu system under different reaction conditions illustrate how dynamic can be the behavior of an inverse oxide/metal catalysts during CO₂ hydrogenation. Small nanoparticles of an oxide on top of a metal substrate can adapt their structure and oxidation state in response to reactant molecules (CO₂, H₂, CO₂/H₂) in extreme ways not seen for a bulk oxide or a conventional metal on oxide configuration. This special behavior leads to high catalytic performance and can be used to design thoroughly efficient catalysts.

CONCLUSIONS

Nanoparticles of ceria deposited on a powder of CuO display a very high selectivity for the production of methanol via CO₂ hydrogenation. CeO₂/CuO catalysts with ceria loadings of 5, 20, and 50% were investigated. Among these, the system with 5% CeO_x showed the best catalytic performance at temperatures between 200 and 350 °C. In-situ studies with XANES and XRD pointed to a full conversion of CuO into metallic copper with an almost complete transformation of Ce⁴⁺ into Ce³⁺. Images of E-TEM showed drastic changes in the morphology of the 5% CeO_x/Cu catalyst when it was exposed to H₂ and CO₂/H₂ mixtures. Under a CO₂/H₂ feed, there was a redispersion of the ceria particles that was detected by E-TEM and in-situ TR-XRD. These

morphological changes were made possible by the inverse oxide/metal configuration and facilitate the binding and conversion of CO₂ to methanol.

DECLARATION OF INTERESTS

The authors declare no competing interests.

SUPPORTING INFORMATION

Activity and selectivity plots as a function of temperature and time. Post-reaction catalyst characterization with XPS. Standards for XANES. Analysis of Ce _{L-III} XANES spectra. In-situ XRD for CO₂ adsorption. STEM and E-TEM images for the catalysts.

ACKNOWLEDGMENTS

The work done at the Chemistry Division of BNL was supported by the U.S. Department of Energy, Office of Science, Office of Basic Energy Sciences, and Catalysis Science Program under contract No. DE-SC0012704. J.A.R. and J.M. received funding from a DOE Office of Science Distinguished Scientist Fellow Award. X.C. and G.Z acknowledge the support by the National Science Foundation (NSF) under DMR 1905422. A.M.A. is grateful for the financial support by Ministerio de Ciencia e Innovación projects RTI2018-101604-B-I00 and PID2021-128915NB-I00. The microscopy studies were carried out using the resources of the Center for Functional Nanomaterials (CFN), a U.S. Department of Energy Office of Science User Facility located at BNL and operated under Contract No. DE-SC0012704. The XAS measurements were performed at beamline 7-BM (QAS) of the National Synchrotron Light Source II, a U.S. DOE Office of

Science User Facility operated for the DOE Office of Science by BNL under Contract No. DE-SC0012704. The QAS beamline operations were supported in part by the Synchrotron Catalysis Consortium (U.S. DOE, Office of Basic Energy Sciences, Grant No. DE-SC0012335). The XRD studies were done at the 17-BM-B (XSD-SRS) beamline of the Advanced Photon Source (APS) in Argonne National Laboratory (ANL), a U.S. DOE Office of Science User Facility operated for the DOE Office of Science by ANL under Contract No. DE-AC02-06CH11357. The authors are grateful to J.R. Balcells for helping with the high-pressure studies.

REFERENCES

¹ D'Alessandro, D. M.; Smit, B.; Long, J. R. Carbon dioxide capture: prospects for new materials. *Angew. Chem. Int. Ed. Engl.* **2010**, *49* (35), 6058-6082. DOI: 10.1002/anie.201000431

² Olah, G. A. Beyond Oil and Gas: The Methanol Economy. *Angew. Chem. Int. Ed.* **2005**, *44* (18), 2636-2639. DOI: 10.1002/anie.200462121

³ Lunkenbein, T.; Schumann, J.; Behrens, M.; Schlögl, R.; Willinger, M. G. Formation of a ZnO Overlayer in Industrial Cu/ZnO/Al₂O₃ Catalysts Induced by Strong Metal-Support Interactions. *Angew. Chem. Int. Ed.* **2015**, *54* (15), 4544-4548. DOI: 10.1002/anie.201411581

⁴ Huang, X.; Beck, A.; Fedorov, A.; Frey, H.; Zhang, B.; Klötzer, B.; van Bokhoven, J. A.; Copéret, C.; Willinger, M.-G. Visualizing Structural and Chemical Transformations of an Industrial Cu/ZnO/Al₂O₃ Pre-catalyst during Activation and CO₂ Reduction. *ChemCatChem* **2022**, *14* (24), e202201280. DOI: 10.1002/cctc.202201280

⁵ Graciani, J.; Mudiyanselage, K.; Xu, F.; Baber, A. E.; Evans, J.; Senanayake, S. D.; Stacchiola, D. J.; Liu, P.; Hrbek, J.; Sanz, J. F.; et al. Highly active copper-ceria and copper-ceria-titania catalysts for methanol synthesis from CO₂. *Science* **2014**, *345* (6196), 546-550. DOI: 10.1126/science.1253057.

⁶ Kattel, S.; Ramirez, P. J.; Chen, J. G.; Rodriguez, J. A.; Liu, P. Active sites for CO₂ hydrogenation to methanol on Cu/ZnO catalysts. *Science* **2017**, *355* (6331), 1296-1299. DOI: 10.1126/science.aal3573.

⁷ Rui, N.; Shi, R.; Gutiérrez, R. A.; Rosales, R.; Kang, J.; Mahapatra, M.; Ramírez, P. J.; Senanayake, S. D.; Rodriguez, J. A. CO₂ Hydrogenation on ZrO₂/Cu(111) Surfaces: Production

- of Methane and Methanol. *Ind. Eng. Chem. Res.* **2021**, *60* (51), 18900-18906. DOI: 10.1021/acs.iecr.1c03229.
- ⁸ Wu, C.; Lin, L.; Liu, J.; Zhang, J.; Zhang, F.; Zhou, T.; Rui, N.; Yao, S.; Deng, Y.; Yang, F.; et al. Inverse ZrO₂/Cu as a highly efficient methanol synthesis catalyst from CO₂ hydrogenation. *Nat. Commun.* **2020**, *11* (1), 5767. DOI: 10.1038/s41467-020-19634-8
- ⁹ Mehar, V.; Huang, E.; Shi, R.; Rosales, R.; Waluyo, I.; Hunt, A.; Liu, P.; Rodriguez, J.A, Microscopic Investigation of H₂ Reduced CuO_x/Cu(100) and ZnO/CuO_x/Cu(111) Inverse Catalysts: STM, AP-XPS, and DFT Studies, *ACS Catal.* **2023**, *13* (14), 9857-9870. D.O.I. 10.1021/acscatal.3c02514.
- ¹⁰ Rodriguez, J. A.; Liu, P.; Graciani, J.; Senanayake, S. D.; Grinter, D. C.; Stacchiola, D.; Hrbek, J.; Fernández-Sanz, J. Inverse Oxide/Metal Catalysts in Fundamental Studies and Practical Applications: A Perspective of Recent Developments. *J. Phys. Chem. Lett.* **2016**, 7 (13), 2627-2639. DOI: 10.1021/acs.jpclett.6b00499
- ¹¹ Zhang, J.; Medlin, J. W. Catalyst design using an inverse strategy: From mechanistic studies on inverted model catalysts to applications of oxide-coated metal nanoparticles. *Surf. Sci. Rep.* **2018**, 73 (4), 117-152. DOI: 10.1016/j.surfrep.2018.06.002.
- ¹² Hornés, A.; Hungría, A. B.; Bera, P.; Cámara, A. L.; Fernández-García, M.; Martínez-Arias, A.; Barrio, L.; Estrella, M.; Zhou, G.; Fonseca, J. J.; et al. Inverse CeO₂/CuO Catalyst As an Alternative to Classical Direct Configurations for Preferential Oxidation of CO in Hydrogen-Rich Stream. *J. Am. Chem. Soc.* **2010**, *132* (1), 34-35. DOI: 10.1021/ja9089846
- ¹³ Barrio, L; Estrella, M.; Zhou, G.; Wen, W.; Hanson, J.C.; Hungría, A.B.; Hornés, A.; Fernandez-Garcia, M; Martínez-Arias, A.; Rodriguez, J.A. Unraveling the Active Site in Copper-Ceria Systems for the Water-Gas Shift Reaction: In Situ Characterization of an Inverse Powder CeO_x/CuO-Cu Catalyst, *J. Phys, Chem. C*, **2010**, *114* (8), 3580-3587. DOI:10.1021/jp910342b
- ¹⁴ Divins, N. J.; Kordus, D.; Timoshenko, J.; Sinev, I.; Zegkinoglou, I.; Bergmann, A.; Chee, S. W.; Widrinna, S.; Karslıoğlu, O.; Mistry, H.; et al. Operando high-pressure investigation of size-controlled CuZn catalysts for the methanol synthesis reaction. *Nat. Commun.* **2021**, *12* (1), 1435. DOI: 10.1038/s41467-021-21604-7.
- ¹⁵ Senanayake, S. D.; Ramírez, P. J.; Waluyo, I.; Kundu, S.; Mudiyanselage, K.; Liu, Z.; Liu, Z.; Axnanda, S.; Stacchiola, D. J.; Evans, J.; et al. Hydrogenation of CO₂ to Methanol on CeO_x/Cu(111) and ZnO/Cu(111) Catalysts: Role of the Metal–Oxide Interface and Importance of Ce³⁺ Sites. *J. Phys. Chem. C* **2016**, *120* (3), 1778-1784. DOI: 10.1021/acs.jpcc.5b12012.
- ¹⁶ Rui, N.; Zhang, F.; Sun, K.; Liu, Z.; Xu, W.; Stavitski, E.; Senanayake, S. D.; Rodriguez, J. A.; Liu, C.-J. Hydrogenation of CO₂ to Methanol on a $Au^{\delta+}$ –In₂O_{3-x} Catalyst. *ACS Catal.* **2020**, *10* (19), 11307-11317. DOI: 10.1021/acscatal.0c02120.

¹⁷ Zhong, Z.; Etim, U. J.; Song, Y. Improving the Cu/ZnO-Based Catalysts for Carbon Dioxide Hydrogenation to Methanol, and the Use of Methanol as a Renewable Energy Storage Media. *Frontiers in Energy Research*, **2020**, *8*, 545431. DOI: 10.3389/fenrg.2020.545431

- ¹⁸ Cui, X.; Liu, X.; Yan, W.; Xue, Y.; Mei, Y.; Li, J.; Gao, X.; Zhang, H.; Zhu, S.; Niu, Y.; Deng, T. Enhancing Methanol Selectivity of Commercial Cu/ZnO/Al₂O₃ Catalyst in CO₂ Hydrogenation by Surface Silylation, *Applied Catal. B: Environmental* **2023**, *339*, 123099. DOI: 10.1016/j.apcatb.2023.123099.
- ¹⁹ Ouyang, B.; Tan, W.; Bing, L. Morphology effect of nanostructure ceria on the Cu/CeO₂ catalysts for synthesis of methanol from CO₂ hydrogenation. *Catal. Commun.* **2017**, *95*, 36-39. DOI: 10.1016/j.catcom.2017.03.005
- ²⁰ Biesinger, M.C. Advanced Analysis of Copper X-ray Photoelectron Spectra, *Surf. Interface Anal.* **2017**, *49* (8), 1325-1334. DOI: 10.1002/sia.6239.
- ²¹ Mullins, D.R. The Surface Chemistry of Cerium Oxide, *Surf. Sci. Reports*, 2015, 70 (1), 42-85. DOI: 10.106/j.surfrep.2014.12.001.
- Wang, X.; Rodriguez, J.A.; Hanson, J.C.; Gamarra, D.; Martínez-Arias, A.; Fernández-García, M. In Situ Studies of the Active Sites for the Water Gas Shift Reaction over Cu-CeO₂ Catalysts: Complex Interaction between Metallic Copper and Oxygen Vacancies of Ceria, *J. Phys. Chem.* 2006, 110, 428-434. DOI: 10.1021/jp055467g
- ²³ Kim, J.Y.; Rodriguez, J.A.; Hanson, J.C.; Frenkel, A.I.; Lee, P. L. Reduction of CuO and Cu₂O: H Embedding and Kinetic Effects in the Formation of Suboxides, *J. Am. Chem. Soc.* **2003**, *125*, 10684-10692. DOI: 10.1021/ja0301673
- ²⁴ Unutulmazsoy, Y.; Cancellieri, C.; Lin, L.; Jeurgens, L.P.H. Reduction of Thermally Grown Single-phase CuO and Cu₂O Thin Films by In-situ Time-resolved XRD, *Applied Surf. Sci.* **2022**, *588*, 152896. DOI: 10.1016/j.apsusc.2022.152896
- ²⁵ Popov, V.V.; Menuschenkov, A,P.; Khubbutdinov, R.M.; Svetogorov, R.D.; Zubavichus, Y.V.; Sharapov, A.S.; Kurilkin, V.V. Influence of Synthesis Conditions on the Crystal Structure of the Powder Formed in the ZrO₂-Ce₂O₃/CeO₂ System, *J. of Phys.: Conference Series*, **2016**, 747, 012041. DOI: 10.1088/1742-6596/747/1/012041
- ²⁶ Luo, S.; Nguyen-Phan, T.-D. Johnston-Peck, A.C.; Barrio, L.; Sallis, S.; Arena, D.A.; Kundu, S.; Xu, W.; Piper, L.F.J.; Stach, E.A.; Polyansky, D.E.; Fujita, E.; Rodriguez, J.A.; Senanayake, S.D. Hierarchical Heterogeneity at the CeOx–TiO₂ Interface: Electronic and Geometric Structural Influence on the Photocatalytic Activity of Oxide on Oxide Nanostructures, *J. Phys. Chem. C*, **2015**, *119* (3), 2669-2679. DOI: 10.1021/jp511986n

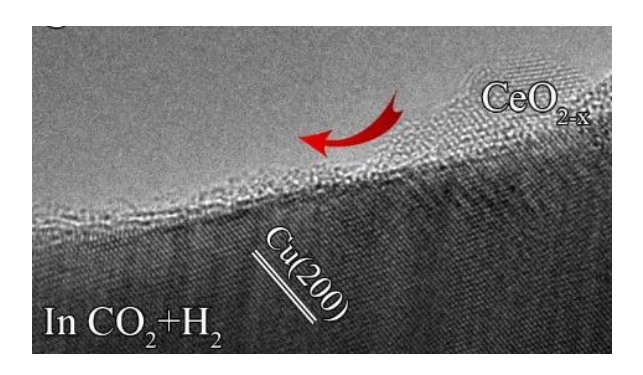
28

²⁷ Albrecht, P. M.; Jiang, D.-e.; Mullins, D. R. CO₂ Adsorption As a Flat-Lying, Tridentate Carbonate on CeO₂(100). *J. Phys. Chem. C* **2014**, *118* (17), 9042-9050. DOI: 10.1021/jp501201b.

²⁸ Kim, K. S.; Barteau, M. A. Reactions of methanol on TiO₂(001) single crystal surfaces. *Surf. Sci.* **1989**, *223* (1), 13-32. DOI: https://doi.org/10.1016/0039-6028(89)90723-1.

- ²⁹ Mullins, D. R.; Robbins, M. D.; Zhou, J. Adsorption and reaction of methanol on thin-film cerium oxide. *Surf. Sci.* **2006**, *600* (7), 1547-1558. DOI: 10.1016/j.susc.2006.02.011.
- ³⁰ Graciani, J.; Grinter, D. C.; Ramírez, P. J.; Palomino, R. M.; Xu, F.; Waluyo, I.; Stacchiola, D.; Fdez Sanz, J.; Senanayake, S. D.; Rodriguez, J. A. Conversion of CO₂ to Methanol and Ethanol on Pt/CeO_x/TiO₂(110): Enabling Role of Water in C–C Bond Formation. *ACS Catal.* **2022**, *12* (24), 15097-15109. DOI: 10.1021/acscatal.2c03823.
- ³¹ Yang, Y.; Mims, C. A.; Mei, D. H.; Peden, C. H. F.; Campbell, C. T. Mechanistic studies of methanol synthesis over Cu from CO/CO₂/H₂/H₂O mixtures: The source of C in methanol and the role of water. *J. Catal.* **2013**, *298*, 10-17. DOI: 10.1016/j.jcat.2012.10.028.
- ³² Wang, J.; Zhang, G.; Zhu, J.; Zhang, X.; Ding, F.; Zhang, A.; Guo, X.; Song, C. CO₂ Hydrogenation to Methanol over In₂O₃-Based Catalysts: From Mechanism to Catalyst Development, *ACS Catal.* **2021**, *11*, 1406–1423. <u>DOI: 10.1021/acscatal.0c03665</u>
- ³³ Beck, A.; Huang, X.; Artiglia, L.; Zabilskiy, M.; Wang, X.; Rzepka, P.; Palagin, D.; Willinger, M.-G.; van Bokhoven, J. A. The dynamics of overlayer formation on catalyst nanoparticles and strong metal-support interaction. *Nat. Commun.* **2020**, *11* (1), 3220. DOI: 10.1038/s41467-020-17070-2.
- ³⁴ Monai, M.; Jenkinson, K.; Melcherts, A.E.M.; Louwen, J.N.; Irmak, E.A.; Van Aert, S.; Altantzis, T.; Vogt, C.; Van der Stam, W. et al. Restructuring of titanium oxide overlayers over nickel nanoparticles during catalysis. *Science*, **2023**, *380*, 644-651, doi:10.1126/science.adf6984.
- ³⁵ Boyes, E. D.; Gai, P. L. Visualising reacting single atoms under controlled conditions: Advances in atomic resolution in situ Environmental (Scanning) Transmission Electron Microscopy (E(S)TEM). *Comptes Rendus Physique* **2014**, *15* (2), 200-213. DOI: https://doi.org/10.1016/j.crhy.2014.01.002.
- ³⁶ Crozier, P. A.; Hansen, T. W. In situ and operando transmission electron microscopy of catalytic materials. *MRS Bull.* **2015**, *40* (1), 38-45. DOI: 10.1557/mrs.2014.304.
- ³⁷ Kim, Y. Y.; Keller, T. F.; Goncalves, T. J.; Abuin, M.; Runge, H.; Gelisio, L.; Carnis, J.; Vonk, V.; Plessow, P. N.; Vartaniants, I. A.; et al. Single alloy nanoparticle x-ray imaging during a catalytic reaction. *Science Advances* **2021**, *7* (40), eabh0757. DOI: 10.1126/sciadv.abh0757
- ³⁸ Rui, N.; Wang, X.; Deng, K.; Moncada, J.; Rosales, R.; Zhang, F.; Xu, W.; Waluyo, I.; Hunt, A.; Stavitski, E.; et al. Atomic Structural Origin of the High Methanol Selectivity over In₂O₃–Metal Interfaces: Metal–Support Interactions and the Formation of a InO_x Overlayer in Ru/In₂O₃ Catalysts during CO₂ Hydrogenation. *ACS Catal.* **2023**, *13* (5), 3187-3200. DOI: 10.1021/acscatal.2c06029.

TOC



³⁹ Kordus, D.; Jelic, J.; Lopez Luna, M.; Divins, N. J.; Timoshenko, J.; Chee, S. W.; Rettenmaier, C.; Kröhnert, J.; Kühl, S.; Trunschke, A.; et al. Shape-Dependent CO₂ Hydrogenation to Methanol over Cu₂O Nanocubes Supported on ZnO. *J. Am. Chem. Soc.* **2023**, *145* (5), 3016-3030. DOI: 10.1021/jacs.2c11540.

⁴⁰ Graciani, J.; Vidal, A.B.; Rodriguez, J.A.; Sanz, J.F. Unraveling the Nature of the Oxide-Metal Interaction in Ceria-Based Noble Metal Inverse Catalysts, *J. Phys. Chem. C*, **2014**, *118* (10), 26931-26938. DOI: 10.1021/jp509947t.

⁴¹ Jia, Y.; Hsu, H.-S.; Huang, W.-C.; Lee, D.-W.; Lee, S.-W.; Chen, T.-Y.; Zhou, L.; Wang, J.-H.; Wang, K.-W.; Dai, S. Probing the Roles of Indium Oxides on Copper Catalysts for Enhanced Selectivity during CO2-to-CO Electrochemical Reduction. *Nano Lett.* **2023**, *23* (6), 2262-2268. DOI: 10.1021/acs.nanolett.2c04925.

⁴² Yang, S.; Liu, Z.; An, H.; Arnouts, S.; de Ruiter, J.; Rollier, F.; Bals, S.; Altantzis, T.; Figueiredo, M. C.; Filot, I. A. W.; et al. Near-Unity Electrochemical CO₂ to CO Conversion over Sn-Doped Copper Oxide Nanoparticles. *ACS Catal.* **2022**, *12* (24), 15146-15156. DOI: 10.1021/acscatal.2c04279.